IEEE Access
Multidisciplinary | Rapid Review | Open Access Journal

Received November 30, 2017, accepted December 27, 2017, date of publication January 9, 2018, date of current version April 23, 2018.

Digital Object Identifier 10.1109/ACCESS.2018.2791429

Performance Analysis and Evaluation for Active Antenna Arrays Under Three-Dimensional Wireless Channel Model

GUODONG LI[1,2], JINSONG WU[3], (Senior Member, IEEE), ZHIXIN CHEN[1,2], XIONG LUO[4,5], (Member, IEEE), TAOLIN TANG[1,2], AND ZHIQIANG XU[1,2]

[1]Fishery Machinery and Instrument Research Institute, Chinese Academy of Fishery Sciences, Shanghai 200092, China
[2]Joint Laboratory for Deep Blue Fishering Engineering and Qingdao National Laboratory for Marine Science and Technology, Qingdao 266000, China
[3]Department of Electrical Engineering, Universidad de Chile, Santiago 8370451, Chile
[4]School of Computer and Communication Engineering, University of Science and Technology Beijing, Beijing 100083, China
[5]Beijing Key Laboratory of Knowledge Engineering for Materials Science, Beijing 100083, China

Corresponding authors: Guodong Li (liguodong@fmiri.ac.cn) and Jinsong Wu (wujs@ieee.org)

This work was supported in part by the Basic Research Foundation of Chinese Academy of Fishery Sciences, Research and Validation of Fishing Vessel Network Architecture, under Grant 2017HY-ZD0801, and in part by the Joint Laboratory for Deep Blue Fishering Engineering and Qingdao National Laboratory for Marine Science and Technology, China.

ABSTRACT In this paper, we establish a full 3-D channel model to support the performance analysis and evaluation of active antenna array (AAA)-based wireless communication systems. We analyze and compare the impact of three different downtilt methods employed in AAA antennas, electrical downtilt (ET), mechanical downtilt (MT), hybrid downtilt (the combination of ET and MT), on the antenna patterns, which would notably impact the performance of mobile wireless communication systems. We compare the performances of the wireless communication system throughput based on the 2-D and 3-D wireless channel models using passive antenna arrays. We also investigate the system performance in terms of the capacity and coverage with different AAAs under the 3-D channel. After the performance analysis and evaluation, we have observed that the downtilt optimization may introduce significant gains in coverage and capacity for individual antennas with smaller beamwidth of the vertical patterns, but may not lead to notable gains for individual antennas with relative larger beamwidth of the vertical patterns.

INDEX TERMS 3-dimensional (3D) channel model, active antenna array, downtilt, beamwidth.

I. INTRODUCTION

For recent years, there have been a number of research and efforts for the 5-th generation (5G) wireless communications systems. To support 5G wireless communications, there have been significant interests in enhancing system performance through the use of active array antenna systems (AAS) having a two-dimensional array structure that provides adaptive control over both the elevation dimension and the azimuth dimension. Active array antenna (AAA) systems, where RF (radio frequency) components such as power amplifiers and transceivers are integrated with an array of antennas elements, offer some benefits compared to traditional deployments with passive antennas connected to transceivers through feeder cables [1]. In the existing research literature for AAA [2]–[5], each antenna was assumed with only one element, while the recent deployments of AASs in communication systems have allowed a variety of new strategies such as the different numbers of elements in an antenna, the different numbers of the vertical and horizontal antennas in AAA, the different spaces between antennas, and so on to balance the system performance and the implementation complexity of the hardware and the algorithms.

The impact of electrical downtilt and mechanical downtilt for passive antenna array (PAA) on LTE (long term evolution) and LTE-Advanced downlink systems has been investigated [5], [6]. As shown in [5], the electrical downtilt may help improve the performance in interference limited systems. According to [6], the choices of tilt methods have not significantly impact the performance of PAA. However, according to the best knowledge of the authors, the impact of downtilts on the performance of AASs, which is the focus of this paper, has not been investigated in literature.

To evaluate the performance of different AAA solutions, it is necessary to establish a full 3-dimensional (3D) channel model in both the horizontal plane and the vertical plane, since the travel of waves in the actual wireless channels are

in both the horizontal plane and the vertical plane. However, the existing channel models, such as SCM [7], WINNER and WINNERII [8]–[10], and ITU [11] ones, are not full 3D models. Although the inclusion of the vertical coordinate component and a 3D representation of antenna arrays are considered and modeled in a few occasions in WINNER and WINNER II channel models [8]–[10], two channel models between the transmitting and receiving arrays remained 2D [9], [10]. The vertical plane is considered in large scale in the current ITU channel model, whereas in small scale elevation angle spread still is zero [9]. Therefore ITU channel model is not a full 3D model. A full 3D channel model could properly simulate actual 3D wireless channels, and AAA should be evaluated based on a full 3D wireless channel model to properly verify 3D beamforming schemes for gaining higher performance.

II. 3D CHANNEL MODEL

A full 3D channel model should include the multipath fading characteristics in both elevation and azimuth planes. The travel of waves in both horizontal and vertical planes are illustrated in Figure 1. Based on the ITU quasi-3D channel model [11], we propose the full 3D wireless channel model, in which elevation are added into the channel model for different scenarios. Two large scale parameters, the elevation angle of departure (EoD) and the elevation angle of arrival (EoA), are added into the 3D channel. Cross-correlation parameters between the two large scale parameters and other five large scale parameters (delay, angle of departure (AoD), angle of arrival (AoA), Shadow Fading standard deviation, Ricean K-factor) are included. The 3D channel coefficient can be written as:

$$\begin{aligned} H_{u,s,n}(t) = \sqrt{p_n} \sum_{m=1}^{M} & \begin{bmatrix} G_{rx,u,V}(\phi_{n,m}, \theta_{n,m}) \\ G_{rx,u,H}(\phi_{n,m}, \theta_{n,m}) \end{bmatrix} \\ & \cdot \begin{bmatrix} \exp(j\Phi_{n,m}^{vv}) & \sqrt{\kappa_{n,m}} \exp(j\Phi_{n,m}^{vh}) \\ \sqrt{\kappa_{n,m}} \exp(j\Phi_{n,m}^{hv}) & \exp(j\Phi_{n,m}^{hh}) \end{bmatrix} \\ & \cdot \begin{bmatrix} G_{tx,u,V}(\varphi_{n,m}, \gamma_{n,m}) \\ G_{tx,u,H}(\varphi_{n,m}, \gamma_{n,m}) \end{bmatrix} \\ & \cdot \exp(j2\pi \lambda_0^{-1} \overline{r_s}.\overline{\Phi}_{n,m}) \\ & \cdot \exp(j2\pi \lambda_0^{-1} \overline{r_u}.\overline{\Psi}_{n,m}) \exp(j2\pi v_{n,m} t), \end{aligned} \quad (1)$$

where $G_{rx,u,V}$ and $G_{rx,u,H}$ are the antenna element u field patterns for vertical and horizontal polarizations respectively, the parameters $\Phi_{n,m}^{vv}$, $\Phi_{n,m}^{vh}$, $\Phi_{n,m}^{hh}$, $\Phi_{n,m}^{hv}$ are the complex gains of vertical-to-vertical, horizontal-to-vertical, horizontal-to-horizontal, and vertical-to-horizontal polarisations of ray (n, m) respectively, λ_0 is the wavelength, $\overline{r_s}.\overline{\Phi}_{n,m}$ is the projection between the departure wave and Tx antenna array, and $v_{n,m}$ is the Doppler frequency of ray (n, m).

The projection between the departure wave and Tx antenna array is given by a scalar product as follows:

$$\begin{aligned} \overline{r_s} \cdot \overline{\Phi}_{n,m} = {} & x_s \cos\gamma_{n,m} \cos\phi_{n,m} \\ & + y_s \cos\gamma_{n,m} \sin\phi_{n,m} + z_s \sin\gamma_{n,m}, \end{aligned} \quad (2)$$

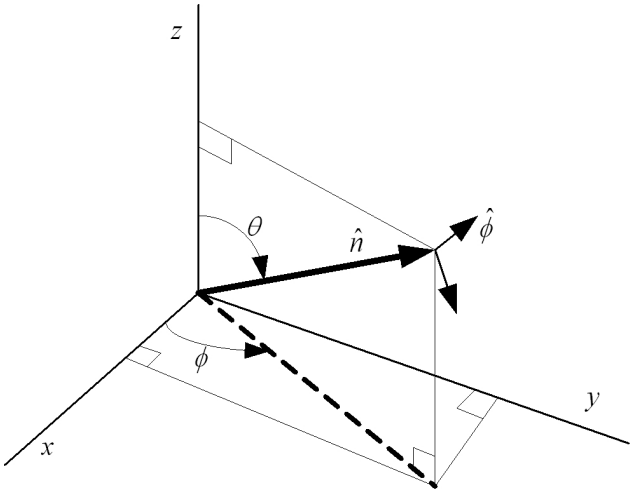

FIGURE 1. Relation between elevation angles and azimuth in 3D channel.

where $\overline{r_s}$ is the location vector of the transmitter array element s, $\overline{\Phi}_{n,m}$ is the departure angle unit vector of the ray (n, m) and x_s, y_s and z_s are components of $\overline{r_s}$ to x, y and z-axis respectively, $\varphi_{n,m}$ and $\gamma_{n,m}$ are the departure azimuth and elevation angles of the ray (n, m) respectively, $\phi_{n,m}$ and $\theta_{n,m}$ are the arrival azimuth and elevation angles of the ray (n, m) respectively. The projection between the incoming wave and the receiving (Rx) antenna array can be defined similarly.

The motion of the mobile terminals is assumed to be in the horizontal direction only for the time being. Then, the Doppler frequency of the nth multipath component can be expressed as

$$v_n = \frac{|\overline{v}|\,[\cos(\varphi_n - \varphi_v)\cos\theta_n]}{\lambda_0}, \quad (3)$$

where $|\overline{v}|$ is the absolute value of the velocity vector of the mobile terminal, the azimuth and the elevation angles of the velocity vector, φ_n and θ_n are, respectively, the azimuth and elevation of the departure/arrival direction of the n-th multipath component at the mobile terminals.

III. ACTIVE ANTENNA ARRAY

A. ACTIVE ANTENNA ARRAY

AAAs can have some advantages compared with the traditional deployments with PAAs. There are a number of different ways in the deployments of AAS in communication systems, such as using different element numbers in antennas, different numbers of vertical and horizontal antennas in AAA, different spaces between antennas, and so on for balancing the system performance and complexity.

The 2D AAS consists of several elements array. In AASs, each individual element array/antenna that consists of a single radiation element or a group of radiation elements has individual Tx(transmitting)/Rx modules in the vertical plane, as shown in Figure 2. In current 3GPP PAA model [12], an element array is equipped with only a TX/RX module with one input port in the vertical direction, as shown in Figure 3.

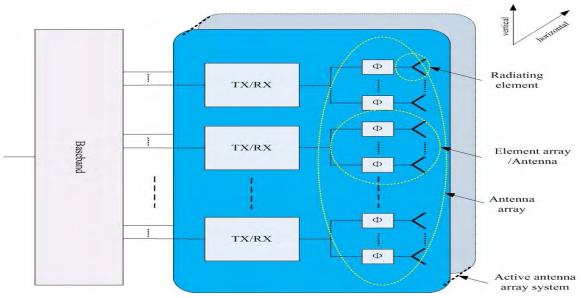

FIGURE 2. Active antenna array.

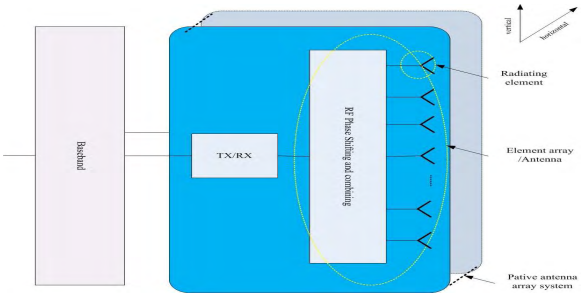

FIGURE 3. Passive antenna array.

All radiating elements in the vertical direction are connected a phase-shifting module and a combining matrix [13].

In AAS, the whole element array field can be formed through multiplying the array factor of the isotropic sources by the field of a single element, as illustrated in Figure 4. The element array factor is given by

$$F_e(\theta) = {W_e}^{\mathcal{H}} a_e(\theta), \tag{4}$$

where the weighting vector ${W_e}^{\mathcal{H}} = [\omega_{e1}, \omega_{e2}, \cdots, \omega_{eN_e}]^{\mathcal{T}}$, $a_e(\theta) = [1, e^{j\frac{2\pi}{\lambda} d_e \sin\theta}, \cdots, e^{j\frac{2\pi}{\lambda}(N_e-1)d_e \sin\theta}]^{\mathcal{T}}$, N_e is the element number of an element array, d_e is the spaces between elements in an element array. The normalization element array factor is given by

$$G_e(\theta) = \frac{|F_e(\theta)|^2}{\max|F_e(\theta)|}. \tag{5}$$

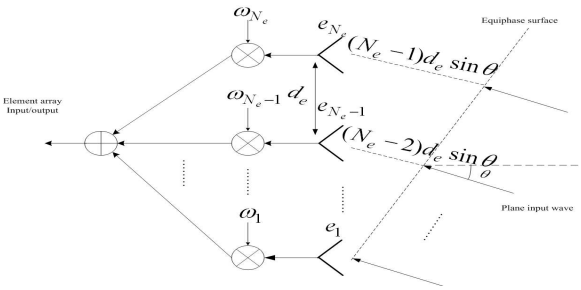

FIGURE 4. Geometry of an antenna array with N_e-elements in far field.

When the element array is the uniform linear array in the vertical plane, the normalization array factor is calculated as

$$G_e(\theta) = \frac{1}{{N_e}^2}\left|\sum_{k=1}^{N_e} e^{j\frac{2\pi}{\lambda}(k-1)d_e \sin\theta}\right|^2 = \left|\frac{\sin(\pi d_e N_e \sin\theta/\lambda)}{N\sin(\pi d_e \sin\theta/\lambda)}\right|^2. \tag{6}$$

B. DIRECTIVITY OF AAA ANTENNA USING DIPOLES

The half-wavelength dipole is one of the most commonly used antennas in wireless communications [13], The vertical radiation pattern for a typical half-wavelength dipole in front of a reflector could be approximated by

$$C_{V\_e}(\theta) = \sin^3(\theta). \tag{7}$$

The horizontal radiation pattern could be approximated by

$$C_{H\_e}(\phi) = -\min\left[12\left(\frac{\phi}{\phi_{3dB}}\right)^2, A_m\right], \tag{8}$$

where A_m is the max attenuation, and ϕ_{3dB} is the 3dB horizontal beam width in the horizontal plane. When an antenna only consists of one element in the horizontal direction, the antenna horizontal pattern could be given by

$$F_{H\_a}(\phi) = C_{H\_e}(\phi), \tag{9}$$

and the antenna vertical pattern is given by

$$F_{V\_a}(\theta) = F_e(\theta) C_{V\_e}(\theta). \tag{10}$$

Then the 3dB main lobe beam width in vertical is defined as

$$D_{3dB} = 10\log\frac{|F_{V\_a}(\theta)|^2}{\max|F_{V\_a}(\theta)|} = -3dB$$

When $N_e = 1, 2, 4, 8$ and $d_e = \lambda/2$, the 3dB main lobe beam width of an antenna in the vertical direction is 54, 28, 14 and 7 degrees respectively. Figure 5 gives the antenna vertical patterns for different numbers of typical half-wavelength dipoles. The gain of the typical half-wavelength Dipole is 8dBi. If the number of elements is doubled, the antenna gain increases by about 3dB.

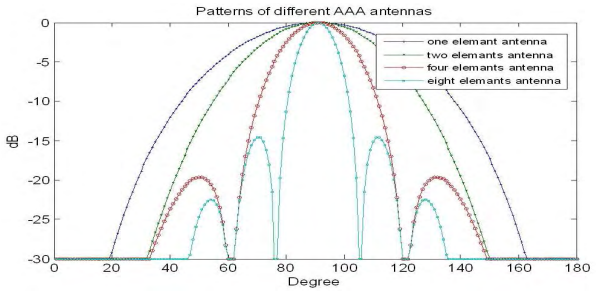

FIGURE 5. Antenna patterns of different AAA antennas.

C. RELATION BETWEEN THE NUMBER OF ELEMENTS AND THE SPACES BETWEEN ANTENNAS

One antenna can consist of a single radiation element or a group of radiating elements in the vertical direction. The length of antenna that consists of half-wavelength dipoles is given as follows

$$L_a = (N_e - 1)d_e + \lambda/2, \tag{11}$$

where d_e denotes the space between elements. We could observe that the space between antennas in the vertical direction is constrained by

$$d_a \geqslant L_a. \tag{12}$$

The AAA array factor is in the vertical direction given by

$$F_a(\theta) = {W_a}^{\mathcal{H}} a_a(\theta), \tag{13}$$

where the weighting vector is ${W_a}^{\mathcal{H}} = [\omega_{a1}, \omega_{a2}, \cdots, \omega_{aN_a}]^{\mathcal{T}}$, $a_a(\theta) = [1, e^{j\frac{2\pi}{\lambda}d_a \sin\theta}, \cdots, e^{j\frac{2\pi}{\lambda}(N_a-1)d_a \sin\theta}]^{\mathcal{T}}$ is the antenna number of an antenna array. The AAA vertical pattern is

$$AF(\theta) = F_a(\theta)F_{V\_a}(\theta) = {W_a}^{H} a_a(\theta){W_e}^{H} a_e(\theta)C_{V\_e}(\theta), \tag{14}$$

where the static or semi-static weighting vector W_e is employed by the electrical downtilt, the weighting vector W_a is used for the real time baseband processing in the TX/RX model. When ${W_e}^{\mathcal{H}} = [1, 1, \cdots, 1]^{\mathcal{T}}$ and ${W_a}^{\mathcal{H}} = [1, 1, \cdots, 1]^{\mathcal{T}}$, (13) is reduced to

$$\begin{aligned} AF(\theta) = {} & [1 + e^{j\frac{2\pi}{\lambda}d_a \sin\theta} + \cdots + e^{j\frac{2\pi}{\lambda}(N_a-1)d_a \sin\theta}] \\ & \cdot [1 + e^{j\frac{2\pi}{\lambda}d_e \sin\theta} + \cdots + e^{j\frac{2\pi}{\lambda}(N_e-1)d_e \sin\theta}]C(\theta). \end{aligned} \tag{15}$$

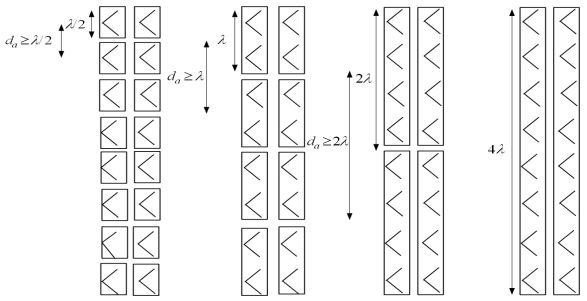

FIGURE 6. The number of elements and the space between antennas.

As shown in Figure 6, the different AAAs are with the same element number, $N_eN_a = K$. When $d_a = L_a$ and $d_e = \lambda/2$, (15) is reduced to

$$\begin{aligned} AF(\theta) &= [1 + e^{j\frac{2\pi}{\lambda}d_e \sin\theta} + \cdots + e^{j\frac{2\pi}{\lambda}(K-1)d_e \sin\theta}]C(\theta) \\ &= [1 + e^{j\pi \sin\theta} + \cdots + e^{j(K-1)\pi \sin\theta}]C(\theta). \end{aligned} \tag{16}$$

An AAA with more individual antennas can achieve the same beam as an AAA with less individual antennas through adjusting the dynamic weighting vector W_a at the cost of more computational complexities in the baseband processing and more RF sources.

IV. EFFECTS OF MECHANICAL AND ELECTRICAL DOWNTILT

Downtilt is a standard feature of mobile communication antennas by adjusting the vertical direction of the main antenna beam. Adjusting downtilt may impact the whole antenna pattern, the antenna gain of the main beam, the beamwidth, and the side lobes. In this section we investigate the mechanical downtilts, electrical downtilts, and the combination of the two methods, which may impact the system performance of AASs.

A. MECHANICAL DOWNTILT

Antenna downtilts could be adjusted mechanically. In MT (mechanical downtilt), the antenna main and side lobes are lowered on one side and the antenna back lobe is raised on the other side because antenna elements are physically directed towards ground. A mechanical downtilt is modeled as the rotation of the antenna-fixed coordinate system around the y-axis (Assume that the AAA is installed in the yoz-plane). This transformation relates the spherical angles (θ, ϕ) in the global coordinate system to spherical angles (θ', ϕ') in the antenna local coordinate system and is defined as follows

$$\theta' = \arccos(\cos\phi \sin\theta \sin\theta_{MT} + \cos\theta \cos\theta_{MT}), \tag{17}$$

$$\phi' = \arg(\tau), \tag{18}$$

where θ_{MT} is the angle value of the mechanical downtilt, $\tau = \cos\phi \sin\theta \cos\theta_{MT} - \cos\theta \sin\theta_{MT} + j \sin\phi \sin\theta$. The total vertical antenna pattern with the mechanical downtilt is given by

$$F_{V\_a}(\theta) = F_{V\_e}(\theta')C_{V\_e}(\theta') \tag{19}$$

The relation between the 3D pattern $G_a(\phi', \theta')$ in the local system and the 3D pattern $G_{a\_MT}(\phi, \theta)$ in the global system is given

$$\begin{aligned} G_{a\_MT}(\phi, \theta) &= G_a(\phi', \theta') \\ &= -\min\left\{-\left[G_{H\_a}\left(\phi'\right) + G_{V\_a}\left(\theta'\right)\right], A_m\right\}, \end{aligned} \tag{20}$$

where $G_{V\_a}\left(\theta'\right) = 10\log\left(\left|F_{V\_a}(\theta')\right|^2 / \max\left|F_{V\_a}(\theta')\right|^2\right)$ and $G_{H\_a}\left(\phi'\right) = 10\log\left(\left|F_{H\_a}(\phi')\right|^2 / \max\left|F_{H\_a}(\phi')\right|^2\right)$. This paper only considers UEs on the horizontal plane, where most of UEs are dropped. When $\theta = \pi/2$, (17) and (18) reduce to

$$\theta' = \arccos(\cos\phi \sin\theta_{MT}), \tag{21}$$

$$\phi' = \arg(\cos\phi \cos\theta_{MT} + j \sin\phi). \tag{22}$$

When ϕ increases from 0 to π and θ increases from $\pi/2 - \theta_{MT}$ to $\pi/2 + \theta_{MT}$, the horizontal radiation pattern of the main beam downtilt effectively shrinks from the main direction and widens the beamwidth as illustrated in Figure 7. Widening the beam width of the horizontal radiation patterns clearly increases the beam overlapping between adjacent sectors that is a major source of inter-sector interference.

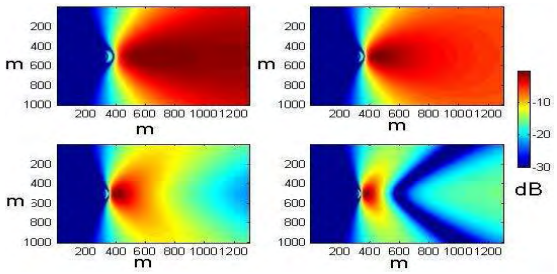

FIGURE 7. Horizontal pattern cuts of mechanical downtilt.

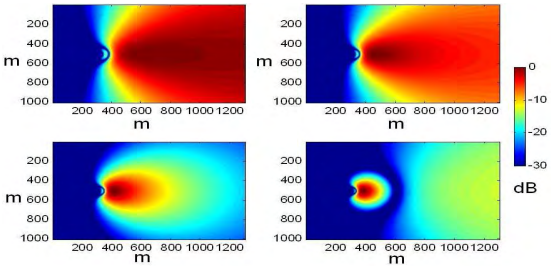

FIGURE 8. Horizontal pattern cuts of electrical downtilt.

B. ELECTRICAL DOWNTILT

The electrical downtilt (ET) is carried out through adjusting electrically. In ET, the main, side, and back lobes are tilted uniformly through adjusting the phases of the antenna elements. When the conventional beamforming (CBF) method is used for adjusting the electrical downtilt, the weighting vector could be [14]

$$W_{CBF} = [1, e^{j\frac{2\pi}{\lambda}d_e \sin\theta_{ET}}, \cdots, e^{j\frac{2\pi}{\lambda}(N-1)d_e \sin\theta_{ET}}]^{\mathcal{T}} \quad (23)$$

where θ_{ET} is value of mechanical downtilt.

The normalized vertical element array factor in (4) can be calculated as:

$$G_{V\_e\_ET}(\theta) == \left|\frac{\sin[\pi d_e N_e(\sin\theta - \sin\theta_{ET})/\lambda]}{N_e \sin[\pi d_e(\sin\theta - \sin\theta_{ET})/\lambda]}\right|^2. \quad (24)$$

The total vertical antenna pattern is given by

$$G_{V\_a\_ET}(\theta) = G_{V\_F\_ET}(\theta) + G_{V\_e}(\theta), \quad (25)$$

where $G_{V\_F\_ET}(\theta) = 10\log\left(G_{V\_a\_ET}(\theta)\right)$ and $G_{V\_e}(\phi') = 10\log\left(\left|C_{V\_e}(\theta)\right|^2 / \max\left|C_{V\_e}(\theta)\right|^2\right)$.

The total pattern $G_{a\_ET}(\phi, \theta)$ is given by

$$G_{a\_ET}(\phi, \theta) = -\min\left\{-\left[G_{H\_a}(\phi) + G_{V\_a\_ET}(\theta)\right], A_m\right\} \quad (26)$$

The maximum values of upper sidelobe occur when

$$\pi d_e(\sin\theta - \sin\theta_{ET})/\lambda = (2m+1)\pi \quad (27)$$

or when

$$\theta_m = \sin^{-1}\left[\frac{\lambda}{\pi d_e}(2m+1)\pi + \sin\theta_{ET}\right], \quad (28)$$

where m is a positive integer. For the vertical antenna pattern in (10), each sidelobe maximum value $G_{V\_F\_ET}(\theta_m)$ of the normalization element array factor does not change with θ_{ET}. Note that $G_{V\_e}\left(\sin^{-1}\left[\frac{\lambda}{\pi d_e}m\pi + \sin\theta_{ET}\right]\right)$ is a monotonously increasing function when θ_{ET} is in $\left[0 : \sin^{-1}\left[\frac{\lambda}{\pi d_e}m\pi\right]\right]$. Thus, $G_{V\_a\_ET}(\theta_m)$ also is a monotonously increasing function when θ_{ET} is in $\left[0 : \sin^{-1}\left[\frac{\lambda}{\pi d_e}m\pi\right]\right]$.

The change of the downtilt angle obviously impacts the 8 elements array radiation characteristics as shown in Figure 8. The electrical downtilt controls the main lobe of the horizontal antenna radiation pattern to minimize the intersector interference and maximize the quality of service within the specified sector. As the main lobe in the vertical plane is tilted down, as illustrated in Figure 9, the upper sidelobes, especially the first upper sidelobe, are raised notably and directed towards the horizon plane, and the sidelobes may create interferences and reduce the system capacity.

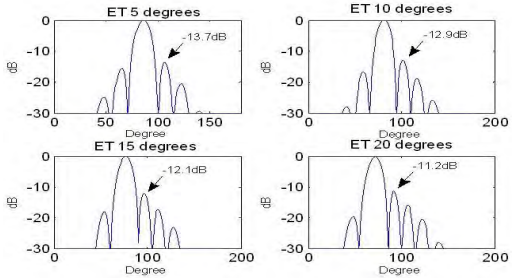

FIGURE 9. Vertical patterns of the AAA which consists of 8 elemants.

Furthermore, the electrical downtilt cannot be deployed in the case of the element array with only one single radiation element. And in the case of a smaller element number of the antenna (such as 2), the elements array radiation characteristics become worse in the vertical plane. The pattern seems acceptable for smaller downtilt changes, while the pattern would become unacceptable larger downtilt.

C. THE COMBINATION OF TWO METHODS

In some scenarios, the electrical downtilt and mechanical downtilt could be jointly employed to improve the system performance. The joint use of electrical and mechanical downtilt may create a big downtilt, which may help reduce intersector interferences introduced by the radiation pattern irregularities of the mechanical downtilt and reduces intercell interferences introduced by the side lobe of the electrical downtilt. From (20) and (26), the total pattern $G_{a\_MT\_ET}(\phi, \theta)$ is given by

$$G_{a\_ET}(\phi, \theta) = -\min\left\{-\left[G_{H\_a}(\phi') + G_{V\_a\_ET}(\theta')\right], A_m\right\}. \quad (29)$$

V. PERFORMANCE

This section provides the system performance results regarding the system capacity and coverage with different AAAs

TABLE 1. Simulation assumptions for antenna and elevation angle of 3D channel.

Parameter	Simulation modeling and values			
AAA model:	2H1V8E	2H2V4E	2H4V2E	2H8V1E
Number of antennas in the horizontal direction	2	2	2	2
Number of antennas in the vertical direction	1	2	4	8
Number of elements in a antenna	8	4	2	1
Spacing between antennas in the vertical direction	_	2λ	λ	0.5λ
Spacing between elements in a antenna	0.5λ	0.5λ	0.5λ	_
Spacing between antennas in the horizontal direction	0.5λ			
Antenna gain	17dBi	14dBi	11dBi	8dBi
Radiating elements	half-wavelength dipole with reflector			
IUT antenna model:	ITU antenna			
Horizontal antenna pattern:	$A_H(\phi) = -\min\left[12\left(\frac{\phi}{\phi_{3dB}}\right)^2, A_m\right]$, where $-180 \le \varphi \le 180, \varphi_{3dB} = 70, Am = 20dB.$			
Vertical antenna pattern:	$A_V(\theta) = -\min\left[12\left(\frac{\theta-\theta_{etilt}}{\theta_{3dB}}\right)^2, SLA_v\right]$, where $-90 \le \theta \le 90, \theta_{3dB} = 10, SLA_V = 20dB$			
3D pattern	$A(\phi,\theta) = -\min\{-[A_H(\phi) + A_V(\theta)], A_m\}$			
Antenna gain	17dBi			
Elevation angle parameter:				
ESD	LOS: $\mu = 0.4\ \sigma = 0.2$; NLOS: $\mu = 0.6\ \sigma = 0.2$			
ESA	LOS: $\mu = 0.6\ \sigma = 0.16$; NLOS: $\mu = 0.88\ \sigma = 0.16$			
Cross-correlations of elevation parameters	LOS and NLOS: ESDvsDS=-0.5; ESDvsASD=0.5; ESDvsASD=0.5 Other cross-correlations is 0			
Main system parameters in Simulation:				
System frequency	2.6G			
System bandwith	20Hz			
Number of cells	19			
Number of sectors in each cell	3			
Channel estimation	ideal			

under the 3D channel obtained through system level simulations based on ITU Scenario uMi. The parameters of AAA antennas and 3D channels are shown in Table 1.

In Figure 10, we compare the performance differences under the 2D channel model (the ITU model) and the 3D channel model proposed in Section II. Meanwhile, in Figure 10, we provide the simulation results using AAA 2H1V8E antenna under the 3D channel model to comparing the system performance between AAA antenna model and ITU antenna model. Figure 10 indicates that coverage performance with ITU antenna under the 2D channel shows better than that under the 3D channel, while the capacity performance with ITU antenna under the 3D channel shows better than that under the 2D channel. Note that that the wave is modeled only in the horizontal plane in the 2D channel model, whereas in the 3D channel model wave is modeled both in the horizontal and the vertical planes. The SNRs of UEs in the cell center become higher under 3D channel, while the SNRs of UEs in cell edge become lower under the 3D channel.

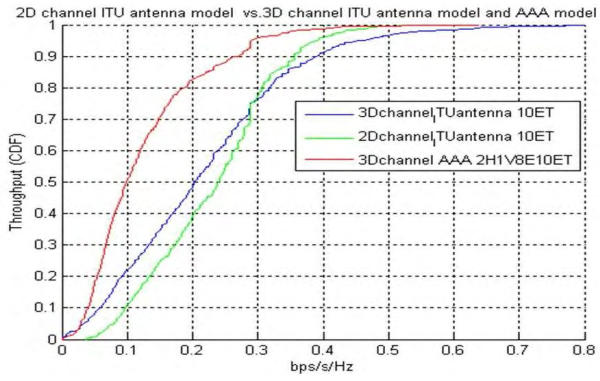

FIGURE 10. Performance for 2D and 3D channel models.

Figure 10 also indicates that system performance using AAA 2H1V8E antenna degrades 40% than that using the ITU antenna model due to the side lobe leakage. Upper side lobe in the AAA antenna model attenuates only 14dB that is higher than the maximal attenuation 20dB in the ITU antenna model assumption.

Different AAA antennas with various downtilts are used to evaluate the system performance under the 3D channel. Figure 11 shows the system performance using the 2H1V8E, 2H2V4E, and 2H4V2E mode antennas with 10 degrees electrical downtilt (10ET, the red curve in the figure), 10 degree mechanical downtilt(10MT, the blue curve in the figure) and combined between 5 degrees electrical downtilt and 5 degrees mechanical downtilt(5ET&5MT, the black curve in the figure). The figure also shows system performance using the 2H8V1E mode antenna with 10 degrees mechanical downtilt.

Figures 11 indicates that the system performances with the increase of individual antenna are improved well, because the antenna gain increases about 3dB when the member of

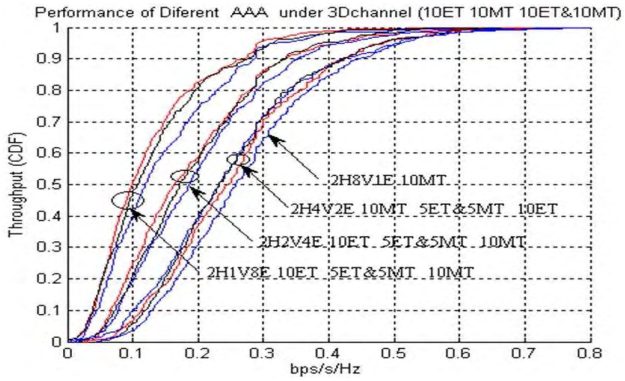

FIGURE 11. Throughput for AAAs with downtilts under 3D channel model.

elements increases double. At the same time, in the case of more individual antennas, more RF hardware resources and higher computational complexities are needed. However, the improvement of the system performance is non-linear to the increase of individual antenna numbers. When the number of individual antennas is a smaller number(such as 2H1V8E and 2H2V4E antennas), the system using the mechanical downtilts outperforms the system using the electrical downtilts in the coverage and the capacity due to the effect of the side lobes of the antenna pattern which leads serious intercell interferences. However, when the number of individual antennas is a relatively large number(such as 2H4V2E), the system using the electrical downtilts outperforms the system using the mechanical downtilts in the coverage and the capacity, since the intercell interferences introduced by the rise of side lobe in ET is weaker than intersector interferences introduced by the radiation pattern irregularities in MT. In this case, the combined downtilt also supports the better performance especially in coverage.

In Figure 12 and 13, the capacity and coverage performances are evaluated using above these different AAAs with various downtilts respectively.

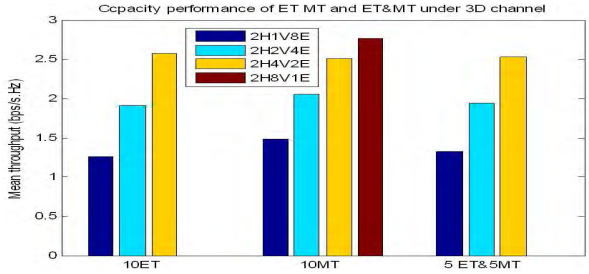

FIGURE 12. Capacity for AAAs with MT, ET, ET&MT in 3D channel model.

In Figures 11, 12, and 13, the system performances are notably improved with the increase of the number of individual antennas. However, more individual antennas may require more RF hardware resources and higher computational complexities. Further, the system performance improvements may be more insignificant when the number of individual

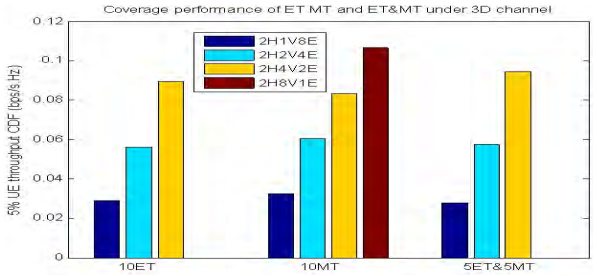

FIGURE 13. Coverage for AAAs with MT, ET, ET&MT in 3D channel model.

antennas is larger. The 2H8V1E antenna system only outperforms the 2H4V2E antenna system by 8%, while the RF hardware resources and computational complexities of the 2H8V1E antenna system are almost doubled those of the 2H4V2E antenna system. In the case that the number of individual antennas(such as 2H1V8E and 2H2V4E antennas) is a small value, both the coverage and the capacity performances using the electrical downtilt are weaker due to the effects of the side lobes which leads to serious intercell interferences. Nevertheless, in the case that the number of individual antennas (such as 2H1V8E and 2H2V4E antennas) is a large value in AAA, the system performance using the electrical downtilt becomes better, since the intercell interferences introduced by the rise of side lobes in the electrical downtilt is weaker than intersector interferences introduced by the radiation pattern irregularities in the mechanical downtilt. In this case, the combined downtilt also supports the better performance especially in coverage.

In the case of the 2H1V8E antenna, the antenna consists of only one radiation element, therefore only the mechanical downtilt can be employed in the system. Figure 14 gives the system performances using the 2H1V8E antenna with the mechanical downtilts 5, 10, 15 and 20 degrees. As observed in Figure 14, different downtilts only have some slight impact on the system performance due to the wider vertical pattern of the antenna in this case.

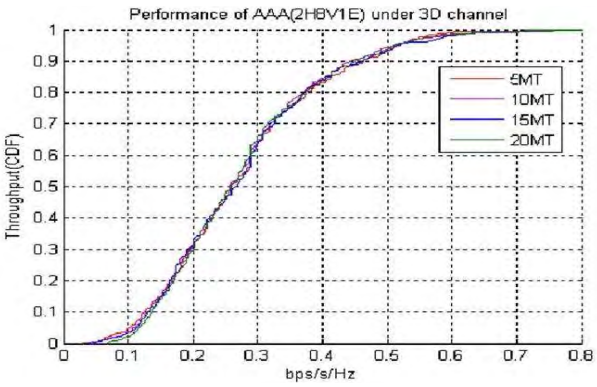

FIGURE 14. Throughput for AAA 2H8V1E in 3D channel model.

In Figure 15, the improvement of the capacity and coverage performance through downtilt optimization is evaluated using

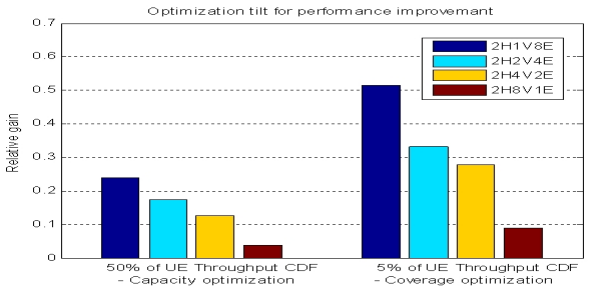

FIGURE 15. Downtilt optimization for AAA performance improvement.

different AAAs with various mechanical downtilts. As shown in Figure 15, the downtilt optimization may introduce significant gains in the case that the number of individual antennas is small, otherwise the downtilt optimization may not be that effective due to the large beam width of the vertical antenna pattern for a large number of individual antennas.

VI. CONCLUSION

In this paper, we have proposed a full 3D channel model method, which could be used in evaluating the performance of AASs. We have analyzed the impact of different downtilts on the AAA antenna patterns. This paper has compared the system performance of different AAAs under between 2D and 3D channel models. We have found that downtilt optimization could introduce significant gains in coverage and capacity for individual antennas with smaller beamwidth of vertical patterns, but could not lead to notable gains for individual antennas with relative larger beamwidth of vertical patterns.

REFERENCES

[1] E. P. Tsakalaki, L. A. M. R. de Temino, T. Haapala, J. L. Roman, and M. A. Arauzo, "Deterministic beamforming for enhanced vertical sectorization and array pattern compensation," in *Proc. 6th Eur. Conf. Antennas Propag. (EUCAP)*, Mar. 2012, pp. 2789–2793.

[2] J. Hyoungju *et al.*, "3D beamforming for capacity boosting in LTE-advanced system," in *Proc. IEEE 26th Annu. Int. Symp. Pers., Indoor, Mobile Radio Commun. (PIMRC)*, Aug. 2015, pp. 2344–2348.

[3] J. Hyoungju *et al.*, "Overview of full-dimension MIMO in LTE-advanced Pro," *IEEE Commun. Mag.*, vol. 55, no. 2, pp. 176–184, Feb. 2017.

[4] O. N. C. Yilmaz, J. Hämäläinen, and S. Hämäläinen, "Vertical sectorization in self-organizing LTE-advanced networks," *Wireless Netw.*, vol. 22, no. 5, pp. 1685–1698, 2016.

[5] N. Phan, T. Bui, H. Jiang, P. Li, Z. Pan, and N. Liu, "Coverage optimization of LTE networks based on antenna tilt adjusting considering network load," *China Commun.*, vol. 14, no. 5, pp. 48–58, 2017.

[6] F. Athley and M. N. Johansson, "Impact of electrical and mechanical antenna tilt on LTE downlink system performance," in *Proc. IEEE 71st Veh. Technol. Conf. (VTC-Spring)*, May 2010, pp. 1–5.

[7] *Spatial Channel Model for Multiple Input Multiple Output (MIMO) Simulations, V10.0.0*, document 3GPP TR 25.996, 2011.

[8] M. Narandzic, C. Schneider, R. Thoma, T. Jamsa, P. Kyosti, and X. Zhao, "Comparison of SCM, SCME, and WINNER channel models," in *Proc. IEEE 65th Veh. Technol. Conf. (VTC-Spring)*, Apr. 2007, pp. 413–417.

[9] J. Meinila *et al.*, *D5.3: WINNERC Final Channel Models*, document CELTIC Project WINNER+ Deliverable, 2010, accessed: Jul. 10, 2017. [Online]. Available: http://projects.celtic-initiative.org/winner+/WINNER+%20Deliverables/D5.3_v1.0.pdf

[10] M. Narandzic *et al.*, "3D-antenna array model for IST-WINNER channel simulations," in *Proc. IEEE 65th Veh. Technol. Conf. (VTC-Spring)*, Apr. 2007, pp. 319–323.

[11] *Guidelines for Evaluation of Radio Interface Technologies for IMT-Advanced*, document Report ITU-R M.2135-1, 2009.

[12] *Further Advancements for E-UTRA Physical Layer Aspects*, document 3GPP TR 36.814 V9.0.0 Release 9, 2010.

[13] 4G Americas. (Jun. 2, 2013). *MIMO and Smart Antennas for Mobile Systems*. Accessed: Jul. 10, 2017. [Online]. Available: http://www.5gamericas.org/files/4614/0622/2152/MIMO_and_Smart_Antennas_July_2013_FINAL.pdf

[14] *Study on RF and EMC Requirements for Active Antenna Array System (AAS) Base Station*, document 3GPP RP-121645 Release 12, 2012.

GUODONG LI received the Ph.D. degree in signal and information processing from the Institute of Acoustics, Chinese Academy of Sciences, Beijing, China, in 2010. He is currently with the Fishery Machinery and Instrument Research Institute, Chinese Academy of Fishery Sciences, Shanghai, China. His research interests include system architecture of 5G wireless communications, massive MIMO, signal processing for multi-carrier systems, and marine communication.

JINSONG WU (SM'11) received the Ph.D. degree in electrical and computer engineering from Queen's University, Kingston, ON, Canada. He is currently an Associate Professor with the Department of Electrical Engineering, Universidad de Chile. His first-authored paper won the 2017 IEEE System Journal Best Paper Award. He received the 2017 IEEE Big Data Technical Committee Best Conference Paper Award, the 2017 IEEE Global Communications Conference (Globecom) Best Paper Award at the Green Communications Systems and Network Symposium, the Best Paper Award at the 2016 IEEE International Conference on Computer Communications International Workshop on Big Data Sciences, Technologies, and Applications, the IEEE Green Communications and Computing Technical Committee 2017 Excellent Services Award from the Excellent Technical Leadership and Services in the Green Communications and Computing Community, and the IEEE Outstanding Leadership Award at the 2013 IEEE International Conference on Green Computing and Communications (Greencom) and at the 2016 IEEE International Conference on Big Data Intelligence and Computing (DataCom), IEEE Computer Society. He is an Elected Vice Chair, Technical Activities, IEEE Environmental Engineering Initiative, a pan-IEEE effort under the IEEE Technical Activities Board. He was the Founder (2011) and the Founding Chair (2011–2017) of the IEEE Technical Committee on Green Communications and Computing (TCGCC). He is also the Primary Co-Founder (2015) and a Founding Vice-Chair of the IEEE Technical Committee on Big Data (TCBD). TCGCC and TCBD are two out of total 26 full technical committees in the IEEE Communications Society with over 65 years history. He was one of the key proposers and a long-term promotor from Green Track to a full green symposium in flagship conferences of the IEEE Communications Society. He opened and established Big Data Track with general and wide topic coverage in the flagship conferences of the IEEE Communications Society, starting at the IEEE Globecom 2016. He was a Symposium Co-Chair and a Track Vice-Chair on Green Communication Systems and Networks of the selected areas in Communications Symposium, IEEE GLOBECOM 2012. He was a Technical Program Committee Chair of the IEEE Online Conference on Green Communications in 2012 and 2013. He was the Leading General Chair of the 2013 IEEE International Conference on Green Computing and Communications. He was a Track Co-Chair on Green Communications and Networks, the IEEE Vehicular Technology Conference in 2014 and 2017.

He was a Leading Proposer and a Co-Chair of the Technical Panels on Big Data for Information and Communication Technologies at the IEEE Globecom 2015. He is a Program Chair of the 2018 IEEE International Environmental Engineering Conference, which is the first edition flagship conference of the IEEE Environmental Engineering Initiative, a multidisciplinary collaboration across the whole IEEE directed to foster knowledge dissemination and innovation in environmental engineering and to promote a sustainable future for the environment. He was the Leading Editor and a co-author of the comprehensive book *Green Communications: Theoretical Fundamentals, Algorithms, and Applications* (CRC Press, 2012), which has been recognized as the very first comprehensive published book effort on green communications covering broad topics of green wireless communications, green wireline communications, general relevant green topics, and applications in one book using a research perspective. He was the very first proposer of the IEEE Green Journals/Transactions (2012). He is the Proposer (2012), Founder (2014), and Series Editor (since 2014) of the IEEE Series on Green Communication and Computing Networks in the *IEEE Communications Magazine*. Since 2016, he has been an Area Editor of the IEEE Transactions on Green Communications and Networking. He was an Original Proposer (2012) and a Series Editor (2014–2016) of the IEEE Journal on Selected Areas in Communications Series on Green Communications and Networking, an Editor of the IEEE Communications Surveys and Tutorials, and an Associate Editor of the IEEE Systems Journal and the IEEE Access.

ZHIXIN CHEN received the B.S. degree from Shanghai Maritime University, Shanghai, China, in 1992, and the M.S. degree from Tongji University, Shanghai, in 2004, respectively. He is currently a Researcher with the Fishery Machinery and Instrument Research Institute, Chinese Academy of Fishery Sciences, Shanghai. His research interests are in the areas of maritime wideband communication networks, ocean engineering, and green wireless communication.

XIONG LUO received the B.Sc. degree in computer science education from Hunan Normal University, Changsha, China, in 1999, and the Ph.D. degree in computer applied technology from Central South University, Changsha, in 2004. From 2004 to 2005, he received the Post-Doctoral Fellowships from Tsinghua University, Beijing, China. From 2012 to 2013, he was a Visiting Scholar with Arizona State University, Tempe, AZ, USA. He is currently a Full Professor with the School of Computer and Communication Engineering, University of Science and Technology Beijing, Beijing. He has published extensively in his areas of interest in journals, such as the IEEE Access, *Future Generation Computer Systems*, *Neurocomputing*, *Computer Networks*, and *Cognitive Computation*. His current research interests include machine learning, cloud computing, and computational intelligence. He received the 2002 IEEE CSS/Beijing Chapter Young Author Best Paper Award.

TAOLIN TANG received the B.Sc. degree in telecommunication and information from the Tianjin University of Technology, Tianjin, China, in 1999. In 2002, he became an Associate Researcher with the Fishery Machinery and Instrument Research Institute, Chinese Academy of Fishery Sciences, Shanghai, China. His current research interests include underwater acoustic signal processing, array signal processing, maritime communications, and massive MIMO systems.

ZHIQIANG XU received the B.S. and M.S. degrees in mechatronics engineering from Tongji University, China, in 2006 and 2009, respectively, where he is currently pursuing the Ph.D. degree in mechatronics engineering. He was an Associate Researcher with the Fishery Machinery and Instrument Research Institute, Chinese Academy of Fishery Sciences, Shanghai, China, in 2009. His current research interests include intelligent control, computer networks, and dynamic systems.